Multispacecraft observation of magnetic cloud erosion by magnetic reconnection during propagation

A. Ruffenach, B. Lavraud, M. J. Owens, J.-A. Sauvaud, N. P. Savani, A. P. Rouillard, P. Démoulin, C. Foullon, A. Opitz, A. Fedorov, et al.

Multi-spacecraft observation of magnetic cloud erosion by magnetic reconnection during propagation

A. Ruffenach,[1,2] B. Lavraud,[1,2] M. J. Owens,[3] J.-A. Sauvaud,[1,2] N. P. Savani,[4,5] A. P. Rouillard,[1,2] P. Démoulin,[6] C. Foullon,[7] A. Opitz,[1,2] A. Fedorov,[1,2] C. J. Jacquey,[1,2] V. Génot,[1,2] P. Louarn,[1,2] J. G. Luhmann,[8] C. T. Russell,[9] C. J. Farrugia,[10] and A. B. Galvin, [10]

[1] Institut de Recherche en Astrophysique et Planétologie, Université de Toulouse (UPS), France
[2] Centre National de la Recherche Scientifique, UMR 5277, Toulouse, France
[3] Space Environment Physics Group, University of Reading, UK
[4] University Corporation for Atmospheric Research (UCAR), Boulder, USA
[5] NASA, Goddard Space Flight Center
[6] Observatoire de Paris, LESIA, UMR 8109 CNRS, 92195 Meudon, France
[7] Centre for Fusion Space and Astrophysics, University of Warwick, UK
[8] Space Sciences Laboratory, UC Berkeley, USA
[9] IGPP/UCLA, Los Angeles, USA
[10] Space Science Center, University of New Hampshire, Durham, New Hampshire, USA

Abstract. During propagation, Magnetic Clouds (MC) interact with their environment and, in particular, may reconnect with the solar wind around it, eroding away part of its initial magnetic flux. Here we quantitatively analyze such an interaction using combined, multi-point observations of the same MC flux rope by STEREO A, B, ACE, WIND and THEMIS on November 19-20, 2007. Observation of azimuthal magnetic flux imbalance inside a MC flux rope has been argued to stem from erosion due to magnetic reconnection at its front boundary. The present study adds to such analysis a large set of signatures expected from this erosion process. (1) Comparison of azimuthal flux imbalance for the same MC at widely separated points precludes the crossing of the MC leg as a source of bias in flux imbalance estimates. (2) The use of different methods, associated errors and parametric analyses show that only an unexpectedly large error in MC axis orientation could explain the azimuthal flux imbalance. (3) Reconnection signatures are observed at the MC front at all spacecraft, consistent with an on-going erosion process. (4) Signatures in suprathermal electrons suggest that the trailing part of the MC has a different large-scale magnetic topology, as expected. The azimuthal magnetic flux erosion estimated at ACE and STEREO A corresponds respectively to 44% and 49% of the inferred initial azimuthal magnetic flux before MC erosion upon propagation. The corresponding average reconnection rate during transit is estimated to be in the range 0.12-0.22 mV/m, suggesting most of the erosion occurs in the inner parts of the heliosphere. Future studies ought to quantify the influence of such an erosion process on geo-effectiveness.

1. Introduction

The interplanetary manifestations of solar coronal mass ejections, called interplanetary coronal mass ejections (ICMEs), are magnetized plasma structures that play a pivotal role in solar-terrestrial interaction [*Gosling* 1993; *Wimmer Schweingruber et al.*, 2006; *Borovsky and Denton*, 2006; *Foullon et al.,* 2007; *Gopalswamy et al*., 2007; *Lavraud and Borovsky*, 2008; *Möstl et al*., 2010; *Richardson and Cane*, 2010]. These structures may interact in various ways with the ambient solar wind during their propagation in the interplanetary medium [*Burlaga et al*., 1987; *Farrugia et al.,* 1997]. Magnetic clouds, a subset of ICMEs, are primarily characterized by a large smooth rotation of enhanced magnetic field, low temperature and low plasma beta [*Burlaga et al.,* 1981; *Klein and Burlaga*, 1982]. The large-scale structure of a MC consists of a twisted magnetic flux rope [*Goldstein*, 1983; *Marubashi*, 1986; *Burlaga*, 1988; *Lepping et al.,* 1990]. Another signature commonly associated with ICMEs is the presence of counterstreaming suprathermal electrons [*Gosling et al.*, 1987; *Farrugia et al.*, 1993] which indicates a large-scale "closed" magnetic topology, with magnetic field lines rooted on the Sun at both ends.

Magnetic reconnection converts magnetic energy into thermal and kinetic energy. Although this process has been mainly studied in situ in Earth's magnetosphere, signatures of magnetic reconnection have previously been associated with magnetic clouds [*Farrugia et al.*, 2001] and confirmed recently as ubiquitous in the solar wind [*Gosling et al.,* 2005a; 2006a; *Davis et al*., 2006; *Phan et al.,* 2006; *Huttunen et al*., 2008; *Lavraud et al*., 2009; *Eriksson et al*., 2009]. *Gosling et al*. [2005a; 2006a] identified Petschek-like reconnection exhausts characterized by bifurcated current sheets. These current sheets form a pair of rotational discontinuities with correlated changes in the components of the magnetic field and flow velocity on one side and anti-correlated changes on the other. Magnetic reconnection implies a change in magnetic field topology. This can be diagnosed using suprathermal electron characteristics since they travel extremely fast along the magnetic field. Unidirectionnal electron beams of a few hundred eV (called the "strahl") are associated with regular solar wind, i.e., open field lines connected to the hot coronal source at one end. Counterstreaming suprathermal electrons, in addition to being observed inside ICMEs [e.g., *Shodhan et al.*, 2000], have been measured in narrow reconnection exhaust at the Heliospheric Current Sheet (HCS). This is also a result of the newly closed nature of the magnetic field lines in the specific configuration of the HCS [*Gosling et al*., 2006b; *Lavraud et al*., 2009] if the spacecraft is crossing the exhaust Sunward of the reconnection line along the magnetic field. By contrast, a spacecraft crossing the exhaust anti-Sunward of the reconnection line observes a lack of strahl electrons in both the parallel and anti-parallel directions [*Gosling et al*., 2005b]. Note that other suprathermal electron signatures have been reported [e.g. *Gosling et al*., 2002; *Steinberg et al*., 2005; *Wimmer-Schweingruber et al.,* 2006; *Skoug et al*., 2006; *Foullon et al.,* 2009; *Lavraud et al*., 2010].

During its propagation in the interplanetary medium, a MC may interact with the solar wind around it. Magnetic reconnection may in particular occur at the front of the MC, thereby leading to a global topological change as depicted in Figure 1. Figure 1 presents the expected magnetic structure as an observing spacecraft would cut through either a non-eroded (panel a) or eroded MC (panel c). *Dasso et al.* [2006] presented a new method to analyze the structure of a MC that consists in calculating the azimuthal magnetic flux accumulated along the spacecraft trajectory. An imbalance in accumulated azimuthal flux, with an excess flux at the back of the MC, is believed to be the signature of magnetic erosion at its front (cf. section 4 for further explanations). This possibility has further been studied using both observations [*Dasso et al.*, 2007; *Möst et al.*, 2008] and global MHD simulations [Schmidt and Cargill, 2003; Taubenschuss et al., 2010]. The simulation works showed in particular that the efficiency of the reconnection process increases with the

relative velocity of the MC with respect to the ambient solar wind.

ICMEs are major sources of strong southward interplanetary magnetic field and often increased solar wind flow speed impinging on the Earth's magnetosphere. The subsequent coupling and geomagnetic storms, mediated in its most part through magnetic reconnection at the dayside magnetopause [*Dungey*, 1961; *Akasofu*, 1981], are directly related to the intensity of the magnetic field in MCs and their sheath regions. Because the proposed erosion directly alters the amount and duration of the typically large magnetic flux contained within MCs impinging on Earth, this process may significantly impact the geo-effectiveness of MCs over the solar cycle. Evaluation of MC magnetic flux budget is also very relevant to the study of coronal processes during eruption [*Qiu et al.*, 2007]. For instance, MC flux estimations are important for comparison with the magnetic flux observed in the suspected solar source region, and which may be used to link MCs to their solar origin [e.g. *Mandrini et al.*, 2005; *Nakwacki et al.*, 2011]. It is thus important to take into account the presumed eroded flux when comparing in situ and solar observations of MCs.

Finally, it should be noted that we use a twisted flux rope hypothesis for our MC in the present study [e.g., *Burlaga,* 1981]. Although this hypothesis appears justified from the results of our multi-spacecraft analysis, MCs have also been described using writhed and sheared three-dimensional magnetic field or spheromak-shaped structures [e.g. *Al Haddad et al.*, 2011; *Vandas et al*, 1993].

Here we study an event that occurred on November 19-21, 2007. The MC was observed by STEREO A (ST-A), STEREO B (ST-B), ACE, WIND and THEMIS in particular. Several authors have studied this event in other contexts [*Gosling and Szabo*, 2008; *Farrugia et al.*, 2011; *Kilpua et al.*, 2011; *Howard and Tappin*, 2009], as will be discussed in section 5. The purpose of the present study is to demonstrate the occurrence of magnetic flux erosion by magnetic reconnection at the front of this MC, owing to its interaction with the slow solar wind ahead of it, using a combination of different methods and signatures together with detailed error assessments. In section 3, we describe data observed by ST-A, ST-B, ACE, WIND and THEMIS. In section 4 we present the different methods used and associated results. We discuss these results in section 5.

2. Instrumentation

The solar terrestrial relations observatory (STEREO) [*Kaiser et al.,* 2008] consists of two spacecraft that slowly drift ahead (referred to ST-A) and behind (referred to ST-B) the Earth on similar orbits around the Sun. The mission was designed to study the solar activity stereoscopically and the structure of the solar wind. We use data from the two Solar Wind Electron Analysers (SWEA) [*Sauvaud et al.,* 2008] and magnetometers (MAG) [*Acuña et al.*, 2008] from the In-situ Measurement of Particles and CME Transient (IMPACT) instrument suite [*Luhmann et al.*, 2008]. Proton data from the PLASTIC instrument [*Galvin et al*., 2008] are also utilised. These instruments are identical onboard each of the two STEREO spacecraft. The time resolutions are 3 seconds and 1 minute for magnetic field and velocity, respectively.

In addition, we make use of measurements from the Advanced Composition Explorer (ACE) spacecraft [*Stone et al.*, 1998], in particular data from the Solar Wind Electron, Proton, Alpha Monitor investigation (SWEPAM) [*McComas et al.*, 1998] and magnetic field (MAG, 3-sec resolution) [*Smith et al.,* 1998]. Due to the low time resolution of ACE velocity moments (1-min resolution), we also use THEMIS-B magnetic field and plasma data (3-sec resolution for both datasets) from the fluxgate magnetometers (FGM) [*Auster et al.*, 2008] and the electrostatic analyzers (ESA) [*McFadden et al.*, 2008].

We work mainly in the RTN coordinate system. This system is centred on the spacecraft, **R** is the sun-to-spacecraft unit vector, **T** is perpendicular to it and points in the direction of planetary/spacecraft orbital motion, **N** completes the right-handed triad. In Figure 10, we use the Heliocentric Earth Ecliptic (HEE) coordinate system where **X** is the Sun-Earth line direction, **Z** is directed towards the North Pole relative to the ecliptic plane and **Y** closes a right-handed system. Electron pitch angle distributions (PADs) at 250 eV are used for ST-A and ST-B. ACE electron PADs are from the 272 eV channel.

3. Overview of the event

The MC under study was observed at 4 main locations: ST-A, ST-B, ACE (L1), and THEMIS (near-Earth environment) (Figure 2). At this time, ST-A and ST-B were separated by ~40° (respectively ~20° west and east from Earth).

Figure 3 shows data from ST-B, ACE, and ST-A. The panels are the same for each spacecraft. The first panel shows the traditional suprathermal electron PAD spectrograms, while the second panel shows the same data but normalised (between 0 and 1) for each sample in time. This allows a better visualisation of PAD characteristics when the dynamic range of fluxes is large. The following panels show ion and magnetic field data in the same format for each spacecraft. The magnetic cloud at ST-B is more complex, we thus first describe below the data from ACE and ST-A.

The magnetic cloud front and back boundaries at ACE are defined at 22:22 UT (Nov. 19) and 11:42 UT (Nov. 20). The magnetic field is high and shows a clear smooth rotation over a large angle inside the MC (panel j). Based on magnetic field data alone, *Gosling and Szabo* [2008] marked the start of the MC at 23:32 UT (Nov. 19) at WIND (corresponding to 23:13 UT at ACE). Based on the magnetic field, plasma and electron PAD data, however, we believe the MC front is observed earlier, at 22:22 UT at ACE (cf. section 4.1.4). Both fronts are marked in Figure 3. Note, however, that this choice does not affect the results regarding azimuthal flux imbalance as discussed in the following sections (the amount of azimuthal flux between these two fronts is small compared to the flux rope magnetic flux, about 5%).

Panel h shows the proton temperature and density for ACE. From 22:22 UT (19 Nov.) to 11:42 UT (20 Nov.), the proton temperature is lower than in the ambient solar wind, again as expected for a MC. The velocity (panel i) is relativity constant, ~ 460 km/s, until 11:42 UT (20 Nov.), only about 70 km/s faster than the solar wind ahead of it. The solar wind velocity enhances significantly after the MC, highlighting the presence of a high speed stream just adjacent and following the MC.

At ACE, before 21:21 UT on 19 November the electron PAD shows a 180° strahl (toward sector) (panel f and g). Just after this time, the PAD becomes field-aligned (0°), indicative of the crossing of the HCS. Counterstreaming electrons appear at 22:22 UT on 19 November implying closed magnetic field lines at the beginning of the MC. From 4:05 UT to 11:42 UT on 20 November, the spectrogram shows unidirectional PADs again; this interval includes essentially the entire second-half (trailing) of the MC.

The duration of the MC at ST-A is longer than at ACE. The MC is characterized by enhanced magnetic field and a clear large-scale rotation of that field between 22:00 UT (19 Nov.) to 3:20 UT (21 Nov.) (panel o). ST-A observes bidirectional suprathermal electrons from 22:00 UT (19 Nov.) to 12:00 UT (20 Nov.) (panel k and l). Unidirectional electrons are yet observed in the trailing part from 12:00 UT (20 Nov.) to the end of the MC at 3:20 UT (21 Nov.). Unlike at ACE, no HCS crossing is observed before the MC. The MC appears to have replaced the HCS at ST-A.

At ST-B, the time period 22:47 UT (19 Nov.) - 7:00 UT (20 Nov.) shows a somewhat

lower proton temperature with an enhanced and rotating magnetic field consistent with signatures of MCs (panel c), apart from a relatively extended and complex region in its middle around 3:00 UT (20 Nov.). Suprathermal electron PADs are mostly unidirectional and in the same direction as at ACE and ST-A (panel a and b), consistent with ST-B sampling the same MC. Based on various in-situ properties, the event at ST-B has been identified as the same event as observed at ACE and ST-A [*Farrugia et al*., 2011; *Kilpua et al*., 2011].

4. Method and erosion signatures

To determine whether magnetic erosion occurs through magnetic reconnection at the front of the MC, we here explore several methods and signatures.

4.1 Magnetic flux imbalance estimation

4.1.1 The direct method of Dasso et al. [2006]

We first employ the "direct method" developed by D*asso et al.* [2006]. This method consists in calculating and analysing the accumulated azimuthal magnetic flux along the spacecraft trajectory in the MC frame. The accumulative flux per unit length is defined as:

$$\frac{F_y(x)}{L_{in}} = \int_{t_{in}}^{t(x)} B_{y,cloud}(t') * V_{x,cloud} dt' \qquad (1)$$

Here t_{in} is the time of the MC front boundary. B_y and V_x are the respective components of the magnetic field and velocity from the observed time series in the MC frame. We use the frame as defined in *Dasso et al.* [2006]. In the RTN coordinate system, the latitude angle θ ([-90°, 90°]) is defined between the ecliptic plane and the cloud axis (called $\boldsymbol{z_{cloud}}$). The longitude angle φ ([-180°, 180°]) is defined as the angle between the projection of the axis in the ecliptic plane and the Sun-spacecraft direction. The direction **d** is defined by the rectilinear trajectory of the spacecraft ($\boldsymbol{-x_{rtn}}$), $\boldsymbol{y_{cloud}}$ is in the direction $\boldsymbol{z_{cloud}} \times \boldsymbol{d}$ and $\mathbf{x_{cloud}}$ completes the right-handed orthonormal base $\boldsymbol{(x_{cloud}, y_{cloud}, z_{cloud})}$. This frame is depicted in Figure 1.

Figure 1 shows an idealized schematic of the expected magnetic configuration for both non-eroded (panel a) and eroded (panel c) MCs, together with the associated variation in each magnetic field component (panels b and d). For non-eroded MCs (panel a), the magnetic field azimuthal component *By* (blue curve) is symmetric about the MC center. Starting the integration of the *By* component at the leading MC boundary, the accumulated azimuthal magnetic flux (red curve) goes back to a null value exactly at the MC trailing boundary. If the MC is eroded (panel c) the expected topological changes alter the variation of the azimuthal *By* component. The accumulated azimuthal magnetic flux is then unbalanced: it goes back to a null value before the end of the MC, revealing what *Dasso et al*. [2006] called a "back region". The back region thus corresponds to an excess of azimuthal magnetic flux whose counterpart at the front of the MC has been eroded through magnetic reconnection.

4.1.2 Determination of the MC orientation using Minimum Variance Analysis

Knowledge of the cloud axis orientation is the prime quantity needed to apply this method. To that end, we use two different methods: minimum variance analysis (MVA) [*Sonnerup et Cahill*, 1967] and force-free MC fitting [*Lepping et al.*, 1990]. With MVA, the cloud axis is determined by the intermediate eigenvector [*Bothmer and Schwenn*, 1998]. We apply MVA to normalized magnetic field vector time series in order to avoid the influence of fluctuations in magnetic field magnitude [*Gulisano et al.*, 2007].

In order to assess potential errors on MC axis orientations from MVA, we apply a bootstrap method [*Kawano and Higuchi*, 1995] with 1000 random resamplings of the magnetic field data acquired inside the MC. This resampling is used to quantify the impact of the intrinsic variability of the dataset on the results. We then repeat this for 7 different nested time intervals within the MC separated by 10 minutes: we begin each of the 7 time intervals 10 minutes after the previous and end it 10 minutes before. This enables us to estimate how errors related to the definition of the MC boundaries may affect the resulting axis orientation. Since such sub-intervals containing a properly defined MC should lead to the same axis determination through MVA, this approach allows us to assess errors from possible sub-structures in the MC (for example, compressions at the edges). Note that for the analysis at ACE, although we consider the leading boundary at 22:22 UT on 19 November for the accumulated azimuthal flux balance estimates, we only apply MVA after 23:13 UT owing to unusual fluctuations of the magnetic field during the interval 22:22-23:13 UT.

4.1.3 Determination of the MC orientation using force-free MC fitting

The second method to determine the MC axis orientation and other parameters is a flux rope fitting (FRF) based on a force-free model with least-square minimisation. The force-free model satisfies the equation $\nabla \times B = \alpha B$ [*Goldstein,* 1983; *Marubashi*, 1986], with α = constant [*Burlaga*, 1988; *Lepping et al*., 1990]. *Lundquist* [1950] gave the solution for a cylindrical geometry in an axially symmetric configuration:

$$\begin{array}{ll} \text{(radial)} & B_r = 0 \\ \text{(azimutal)} & B_\varphi = B_0 J_1(\alpha r) \\ \text{(axial)} & B_z = B_0 J_0(\alpha r) \end{array} \qquad (2)$$

Here J_n is the Bessel function of the first kind of order n, B_0 is the strength of the magnetic field at the MC axis and r is the radial distance from the axis. The constant α determines the magnetic field twist of the flux tube. To apply this method, we estimate initial guesses of the following parameters in the MC frame determined by MVA: the helicity (right or left handed), the MC axis orientation (the latitude angle θ and longitude angle φ), and the impact parameter p (distance between the centre of the flux tube and the spacecraft trajectory through the MC, which is approximated for initial guess as <Bx>/<B> (where Bx is computed in the MC frame previously obtained from MVA [*Démoulin and Dasso*, 2009]). Then, we apply a least square fitting method and a first series of iteration to determine the angle θ and φ. When these are determined, we perform another series of iteration to determine the impact parameter p and α.

It is worth mentioning that the MC is compressed at its rear edge by a high-speed solar wind. This restrains its expansion, as shown by a rather constant speed throughout the MC at all spacecraft. Hence we do not take the MC expansion into account for both MC fitting and analysis of magnetic flux imbalance (cf. next section). *Nakwacki et al*. [2008] have shown, anyway, that radial expansion does not strongly affect such calculation.

4.1.4 Results on magnetic flux imbalance

Table 1 summarizes the results obtained from the above analyses. The accumulative azimuthal magnetic flux per unit length Fy/L, which starts at the front MC boundary, is shown in Figure 4 for ST-B, ACE, and ST-A. The solid colored curves show the results obtained for each of the 7 nested time intervals to which MVA is applied (from the full interval, in purple, to the smallest interval in red), and the 1000 curves observed for each color correspond to the results from the bootstrap resamplings. These curves thus highlight

the errors, or variability, of the azimuthal flux accumulation results. The dashed lines show the result using the axis orientation given by the FRF method at each spacecraft. In Table 1, the time of flux balance is given for each spacecraft and for both methods used: FRF and MVA (for MVA analysis the time corresponds to the mean of the 7000 colored curves)

Despite a large set of trials in error assessment and the use of different methods, there is a clear imbalance in flux in every case for both ST-A and ACE. The more complex case of ST-B does not show a clear signature of potential magnetic erosion (Figure 4). This stems from the unusual magnetic structure that is observed between 02:00 and 04:00 UT on 20 November. This structure impacts on the results of MC axis orientation from MVA and FRF, and thus the magnetic flux balance analysis is possibly biased.

We now report some additional tests that are not shown. We performed a second series of analyses where we modified the time interval used (for both MVA and FRF) so as to exclude the back region from the analysis. Indeed, if the MC is asymmetric owing to erosion, the back region constitutes a region of additional flux with no counterpart on the front side of the MC. Although such asymmetry might influence the results from both MVA and FRF (and in turn the flux balance analysis), the use of a shortened MC interval at ACE without the back region yielded results compatible with erosion and with those obtained when the full MC is analysed. The analysis at ST-A using a shortened MC interval without the back region also shows flux imbalance with similar results, but there is substantially less variability in the results when the back region is removed from analysis. Indeed, we note that our MVA analyses yield weak standard deviations in terms of axis orientation at ACE: lower than 2°. At ST-A, the standard deviation is ~6° if the full MC is analysed (Figure 4) and ~2° (not shown) if the back region is removed from analysis. These results are consistent with the work carried out by *Gulisano et al*. [2007] who studied the bias of MVA in the determination of MC axis orientation. They concluded that the orientation is well determined for MC axes close to the ecliptic plane and with reasonably small impact parameters (i.e., spacecraft crossing close to the MC centre) as in the present case.

As mentioned in section 3, we defined the front MC boundary at 22:22 UT (19 November) at ACE, which is earlier than the corresponding start time given in *Gosling and Szabo* [2008] and *Farrugia et al.* [2011] for WIND. Although not shown, quite obviously if one starts the azimuthal flux accumulation in Figure 4 at the later time defined by these authors, then the estimated back region is even more extended (~5% change in total azimuthal flux).

In conclusion, for both ACE and ST-A the combination of several methods and error analyses based on both bootstrap and changes in the MC boundary definitions all concur and are compatible with the existence of a significant excess magnetic flux in the trailing part of the MC, which we further substantiate and interpret in the next sections.

In order to estimate the amount of azimuthal magnetic flux that was eroded from the front of the MC, we compute the total azimuthal flux before reconnection with the ambient solar wind magnetic field ($F_{t,azimuthal}$), which can be determined using solely the second half of the MC from the sum of Fy/L (in absolute value) between the peak in accumulated flux and the end of the MC (Figure 4) [*Dasso et al.*, 2006]. We assume a MC length of $\approx$ 2 AU in order to be consistent with previous works [e. g. *Nackwacki et al.*, 2011]. We obtain $F_{t,azimuthal}$ =3.36x10^{21} Mx for ACE and 5.42x10^{21} Mx for ST-A. The amount of eroded azimuthal flux $F_{e,azimuthal}$ (i.e., equal to the azimuthal flux contained in the inferred back region) is then given by the absolute value of Fy at the end of the MC, $F_{e,azimuthal}$ =1.48x10^{21} Mx at ACE and 2.68x10^{21} Mx at ST-A. The eroded azimuthal magnetic flux corresponds to 44% and 49% of the total, initial azimuthal magnetic flux, respectively at ACE and ST-A

With regards to the axial magnetic flux F_z, we may also calculate it from observations as performed in *Dasso et al.* [2006, 2007]. We assume a circular MC cross section, p=0 and we compute $r = x(t) - x_{center}$ (x is the distance inside the MC in AU, x_{center} corresponds to the center of the MC as defined by the maximum in accumulated azimuthal By magnetic field) Note that we also neglect the axial flux in the core since it only corresponds to a correction of the order $(p/R)^2$ [*Dasso et al.,* 2006]. Following *Dasso et al*. [2006; 2007], the axial flux is calculated as:

$$F_z = 2\pi \int_{tin}^{t(x)} B_{z,cloud}(t')(x(t')-x_{center})V_{x,cloud}(t')dt'$$

From this calculation we obtain the total axial magnetic fluxes, which are $F_{t,axial}$=0.64 x10^{21} Mx at ACE and 0.69 x10^{21} Mx at ST-A. We also find eroded axial magnetic fluxes of $F_{e,axial}$=0.48 x10^{21} Mx at ACE and 0.31 x10^{21} Mx at ST-A. Hence, the amounts of eroded axial magnetic fluxes correspond to 75% and 45% of the total axial fluxes, respectively at ACE and ST-A.

4.2 Parametric study of axis orientation impact on accumulated azimuthal flux

Figure 5 shows a parametric study that highlights the amount of eroded azimuthal magnetic flux as a function of MC axis orientation. Each contour value quantifies the inferred erosion (as defined in Section 4.1.4) when alternative MC orientations are arbitrarily chosen in terms of latitude and longitude at ACE (a) and ST-A (b). The central value corresponds to the mean MC axis orientation from our analysis (cf. Table 1).

Figure 5 demonstrates that only a large error in axis determination (more than 20° for ST-A and more than 10° for ACE), and specifically towards lower latitude only, could explain the imbalance in azimuthal flux. This simple parametric study further and strongly supports the fact that there is an actual azimuthal flux imbalance at both ACE and ST-A, and which we interpret as the signature of magnetic erosion.

4.3 Signatures of magnetic reconnection at the MC front boundary

The erosion mechanism investigated here implies the occurrence of magnetic reconnection at the front of the MC during its propagation. Magnetic reconnection creates rotational discontinuities that are observed as bifurcated current sheets bounding an exhaust [*Farrugia et al.*, 2001; *Gosling et al.*, 2005a; *Gosling and Szabo*, 2008]. During an exhaust crossing, a spacecraft should observe correlated changes in **V** and **B** components at one edge (or current sheet) of the exhaust and anti-correlated changes at the other edge.

Figure 6 shows selected plasma and magnetic field data at different spacecraft when these cross the front boundary of the MC on 19 November. Vertical dashed green lines identify the transition from the solar wind ahead of the MC (to the left) to the MC itself (to the right). As shown by these lines, there are fairly clear bifurcated current sheet signatures (two well separated gradients mainly in either/or the B_t and B_n components) at the three spacecraft shown: ST-B, THEMIS-B, and ST-A. Note that we use THEMIS-B data here because this dataset has a higher time resolution (3 sec) than ACE (1-min for velocity moments) and because WIND has a data gap at this time. THEMIS B is in the pristine solar wind (as confirmed from visual inspection of the particle energy-time spectrograms) close to Earth at this time (GSE coordinates [-9,-29,-9.5] R_E). To confirm that these bifurcated current sheet signatures are bounding reconnection exhausts, i.e., with Alfvénic changes in the velocity components, we perform the Walén test [*Hudson et al.*, 1970; *Paschmann et al.,* 1986]:

$$V_{pre} = V_{ref} \pm \rho_{ref}^{1/2} \times (B/\rho - B_{ref}/\rho_{ref}) / \mu_0^{1/2} \quad (3)$$

Here, V, B, ρ, represent the velocity, magnetic field and density (the pressure anisotropy factor is not accounted here owing to the lack of such data). The subscript "ref" denotes the reference time at the leading or trailing edge of the exhaust in the upstream region, and subscript "pre" denotes the velocity predicted across the region for an exhaust bounded by rotational discontinuities. The positive (negative) sign is chosen for the trailing (leading) edge of the exhaust. The velocities predicted inside the exhausts are shown as colored dashed lines in Figure 6 for ST-A and THEMIS-B. (For context, Figure 7 shows data only around the exhaust seen at ACE and THEMIS-B, confirming it is indeed the same exhaust observed by THEMIS-B at 23:18 UT (Nov. 19). Moreover, we note that despite the low resolution of the proton velocity data at ACE, the expected velocity change (marked "jet" in Figure 7) is also seen at this spacecraft. Based on the velocity at the MC front (~440km/sec) and the distance between ACE and THEMIS (~224 Re) the expected delay is ~54 min, compatible with observations.

In Figure 6 the Walén tests are performed inward from the vertical black dashed lines, which correspond to the reference times used in the application of Equation (1). As can be seen, the test is basically successful for both THEMIS-B and ST-A. From Figure 6, we note the exhausts at THEMIS-B and ST-A have very different durations. The spatial width of the exhaust is estimated to be 9450 km at THEMIS-B, whereas at ST-A it is 6.1×10^5km. This suggests that ST-A is at a significant distance from the reconnection line while THEMIS-B (and ACE) is much closer. For ST-B, a bifurcated current sheet structure akin to that observed at ACE and THEMIS-B is observed at ~22:46 UT (November 19). However, the time resolution of the proton data is insufficient to perform the Walén test at this spacecraft because the exhaust is much thinner at ST-B than at ST-A.

Because the magnetic field component normal to a reconnecting current sheet should be constant for an ideal magnetic reconnection exhaust with a constant guide field, the MVA minimum eigenvector provides the direction normal to the current sheet while putative reconnection line orientations are given by the intermediate eigenvector direction [see, e.g., *Phan et al.,* 2006; *Gosling et al.,* 2007]. Table 2 summarizes the results for the reconnection line orientations obtained at each spacecraft, together with the local magnetic shear and Walen tests results for the exhausts. Figure 8 shows the orientation of the reconnection lines at the three spacecraft. The main feature is that the reconnection lines at all spacecraft have a significant tilt both away from the equator and away from the radial direction to Sun.

4.4 Signature of large-scale topological changes in suprathermal electrons

Finally, we examine the large-scale topological changes that may be expected from the process of magnetic erosion envisaged here (Figure 1). For this purpose we may use suprathermal electrons as tracers (cf. introduction).

The suprathermal electron PADs displayed in Figure 3 show that this MC is characterised by both closed and open field lines, as indicated by the presence of both bi- and unidirectional suprathermal electrons. The unidirectional beams are observed anti-parallel to the magnetic field at all spacecraft, consistent with the spacecraft observing the same MC. The open field lines with unidirectional electrons observed in the core of the MC, before the back region inferred previously, can be associated with the occurrence of interchange reconnection at the Sun as has often been reported [e.g. *Crooker et al*., 2004; *Owens and Crooker*, 2006; *Lavraud et al*., 2011]. Note, however, that such interchange reconnection cannot affect the magnetic structure of the MC observed at 1 AU because information (travelling at the Alfvén speed) does not have enough time to be transmitted to 1 AU.

The back regions of the MC were estimated to span from 9:53 to 11:43 UT (on 20

November) at ACE and from 23:40 to 03:20 UT (on 20-21 Nov.) at ST-A (vertical red lines in Figure 3). Figure 9 shows 5-minute averages of the suprathermal electron pitch angle distributions (PADs) at times just before and just after this expected transition between the core of the MC and the back region for each spacecraft. The time intervals are respectively 9:00-9:05 UT and 10:30-10:35 on 20 Nov. (23:00-23:05 on 20 Nov. and 00:00-00:05 on 21 Nov.) for ACE (ST-A). Clear changes in both phase space density (PSD) values (parallel and anti-parallel) and distribution angular widths are observed upon entry into the back region for both ACE and ST-A. These are suggestive of a different strahl source for the back region of the MC, as discussed next in section 5.4. Changes are also observed near the end of the MC at ST-B, but these are not analysed, nor interpreted, since the azimuthal flux balance analysis is deemed to be biased at this spacecraft, as discussed in section 5.4.

5. Discussion

We here discuss how this combined set of signatures provides significant, additional evidence for the occurrence of magnetic erosion during the propagation of the MC observed on November 19-21, 2007.

5.1. Evidence from multi-point magnetic flux imbalance analyses

The accumulated azimuthal magnetic flux analysis reveals the presence of an excess magnetic flux in the trailing part of the MC at both ACE and ST-A. *Dasso et al.* [2006] devised and used this method with single satellite observations, and without detailed error assessment. In the present study, the MC is observed at 3 different and widely separated spacecraft. This puts constraints on the spatial configuration of the MC. For instance, as shown in *Owens et al*. [2012], passage through the leg of a MC significantly alters the observed magnetic field signatures (e. g. 'double flux rope' signature). Such large alterations of the magnetic field are not seen at ST-A. ST-A is therefore not sampling the leg of the MC. The longer duration of the MC at ST-A may rather reflect a larger expansion of the MC. This is compatible with the observed lower magnetic field strength, the smaller difference between the MC velocity and solar wind ahead of it, and the absence of a shock at ST-A.

The two MC axes obtained for ACE and ST-A are somewhat different (Figure 5), with the latitude of the axis being larger at ST-A. Focusing on the parametric study for ACE in Figure 5, it is very unlikely that the axis orientation at this spacecraft could be wrong by more than 10°, and specifically towards lower latitude, since this would increase the difference with the orientation found at ST-A and since errors on axis orientation are particularly low at this spacecraft. All these results give strong confidence in the finding that the azimuthal magnetic flux is strongly imbalanced at least at ACE, but also at ST-A. The azimuthal magnetic flux contained in the back region is equivalent to the magnetic flux that has been eroded at the front of the MC. According to our calculations, the amount of azimuthal magnetic flux that was eroded from the front of the MC at ACE corresponds to 44% of the total, initial azimuthal magnetic flux measured, i.e., before erosion. This calculation yields 49% at ST-A. Note that *Dasso et al*. [2006, 2007] estimated the amount of eroded azimuthal magnetic flux with the same method for two MCs on 18-20 November 1995 and 9-11 November 2004: the values were respectively 57% and 17%.

We also noted that the trailing edge of the MC is compressed by a high-speed solar wind. This compression is significant, as observed in the magnetic field (Figure 3), and as shown by *Rouillard et al*. [2010] and *Farrugia et al*. [2011] for this MC. Although such MC distortion may impact the MVA and FRF analyses, as mentioned in section 4 the results are similar when the compressed back region is left out of the analyses at both ACE and ST-A. This effect is also not expected to influence the accumulated flux calculation

since magnetic flux is conserved through mere adiabatic compression. Future studies ought, nevertheless, to study uncompressed MCs.

5.2 Evidence from the estimated MC twist after erosion

The force-free fitting method allows us to estimate the MC α parameter. In the force free model, α=2.41 corresponds to a completely poloidal field at the outer MC boundaries (r = 1). We obtain for ACE a value of 2.16 when analyzing the full MC interval (Table 1). We obtain a value of 1.92 when the back region is left out of the analysis, i.e., when analysing the symmetric part of the MC only. We may claim that this is consistent with an eroded MC in the force-free model assumption. However, because we have no knowledge of the initial configuration (in terms of α parameter) of the MC at the time of its initiation at the Sun, this result only provides an additional element but may not be viewed as a strong argument.

5.3 Evidence from the observation of reconnection at the MC front boundary

MC erosion during propagation in the interplanetary medium implies the occurrence of magnetic reconnection at its front boundary, as depicted in Figure 1. As was demonstrated in section 4.3, signatures of reconnection exhausts at the front boundary of the MC were observed at all spacecraft (though with variable uncertainties owing to different time resolutions and exhaust widths). This demonstrates that the expected magnetic reconnection did occur, at least at the position and time of observation, for this particular MC. We note, however, that although magnetic reconnection at the front boundary of the MC is a prerequisite to the erosion mechanism invoked here, it needs not be observed specifically at the spacecraft at the time of observation as long as it did occur at earlier times during propagation. Interestingly, the erosion is observed here for a rather slow MC (~450 km/s). Erosion is, however, expected to be stronger for faster MCs owing to increased compression at the forward shock, with associated increased reconnection rates.

Figure 10 shows the reconnection lines orientations at the MC fronts, deduced from MVA analysis, in the Y-Z_{HEE} plane. The reconnection lines have somewhat different tilt angles at each spacecraft, which is not unexpected owing to the large inter-spacecraft distances and the 3D geometry of a MC that interacts with its environment. Although it is not the purpose of the present study, we note that the reconnection line tilts in the Y-Z plane are large. This brings up the question of whether there is a single or several patchy reconnection lines present along the front of the MC. This is in analogy to the issue of extended versus patchy reconnection at Earth's dayside magnetopause as a function of IMF conditions, and which also depends on complex 3-dimensional geometrical considerations (as further discussed in section 5.5) and on the influence of various processes occurring at the shock and in the sheath.

5.4 Evidence for a different suprathermal electron strahl source

The suprathermal electrons PADs in the MC back regions show clear changes at ACE and ST-A as compared to the core of the MC. Because the erosion process implies large-scale topological changes (Figure 1), we do expect the source of the strahl in the back region to be different from that in the MC core. This is what is observed for both ACE and ST-A at the expected times (within +/- 1 hours). An unexpected signature would be to observe no changes at all in the PADs as the spacecraft enter the inferred back regions.

The observed enhanced magnetic field in the back region and the presence of a trailing high-speed stream (cf. Figure 3) suggest adiabatic compression is occurring. From Liouville's theorem, such an adiabatic compression would result in a larger PAD width of the strahl, but without any increase in absolute phase space density values around 180°. This is opposite to what is observed at the transition between the core of the MC and the inferred back regions, where the phase space density at 180° significantly increases (decreases) at ST-A (ACE) while the PAD width does not change or even decreases at both

spacecraft. The strahl source is thus different in the back regions at both ACE and ST-A.

5.5 Reconnection scenarios and complexity of the 3D global topology

These signatures in the suprathermal electron PADs are thus consistent with a topological change at the front of the MC and subsequent erosion. However, because of the complex topology of the MC and of the possibly patchy reconnection lines, we have no obvious way of knowing where the eroded magnetic field may now connect to in the heliosphere, and whether or not they should be singly or doubly connected to the Sun. Figure 11 illustrates this fact. Figures 11a-b and 11c-d respectively show configurations where reconnection lines with the rough local properties observed at ST-A and ACE are used. Because the magnetic field and suprathermal electron properties at the MC front boundaries are different at ACE and ST-A, as well as in the slow solar wind ahead of it with different sectors being observed at ACE and ST-A (i.e., the strahl is measured at 0° at 22UT on 19 Nov. at ACE and at 180° at 19UT on 19 Nov. at ST-A), the obtained new connectivity inside the MC may have either closed or open magnetic topologies at other locations along the magnetic fields of the MC.

These configurations, however, are over-simplified. Placing both reconnection scenarios into the same picture significantly alters these simple geometries and makes the global 3D topology more complex. This is illustrated in Figure 11e-f where all cases of parallel, anti-parallel or bidirectional suprathermal electrons may be found at various places in the MC depending on where reconnection occurs. Figures 11e-f may not be viewed as realistic either. This is because even more complex configurations can be envisaged if reconnection varies spatially and temporally, and if reconnection occurs along extended lines rather than points as depicted in the figures for sake of simplicity. Adding to this complexity is the fact that part of the MC is likely disconnected from the Sun at one end (left-hand side of MC in all figures) through interchange reconnection in the corona.

In conclusion, we may not attempt to fully explain the characteristics of suprathermal electrons in the MC but simply note that suprathermal electron PADs must change in the back region. We may not know what strahl and PAD properties are to be expected with the new connectivity because we do not know the global 3D topology that follows from such reconnections. This is also why the relative changes in PAD profiles, as observed in Figure 9 (red and blue curves), do not have to be the same at all spacecraft (again, owing to a complex 3D geometry). PAD properties (e.g., at ST-B) may thus not be used alone to study erosion. Future studies ought to investigate this further, for instance through the use of global modelling.

5.6 Inferences for the preferential location and rate of magnetic reconnection during propagation

We note that *Gosling and Szabo* [2008] found a reconnection exhaust at the trailing boundary of the MC (11:46 UT at WIND / 11:42 UT at ACE on 20 November). This likely stems from the compression that occurs as the trailing high-speed stream overtakes the MC. Because this compression is expected to build-up gradually as it propagates in the heliosphere, it is probable that the reconnection process at the trailing boundary has not been much efficient in the inner heliosphere. By contrast, since the Alfvén speed in the solar wind increases as one approaches the Sun [*Fujimoto et al*., 2007; *Lavraud and Borovsky*, 2008], and magnetic reconnection rate scales with the Alfvén speed, we may expect that a significant portion of the magnetic erosion investigated here has in fact occurred in the inner parts of the heliosphere.

From the observed azimuthal magnetic flux erosion and knowledge of the transit time from the Sun, we can estimate the average reconnection rate which prevailed at the front MC boundary during propagation. *Howard and Tappin* [2009] observed this CME from different viewpoints on 15 November at 18:10 UT (by COR2-B), 18:40 UT (by COR2-A)

and 18:50 UT (by LASCO2). We choose the mean value of 18:30 UT. The transit time to ACE (ST-A) is then in the range 99h 54 min to 113h 12min (99h 30min to 128h 50min) using the front and rear boundaries of the MC. We use both times to estimate uncertainties on the average reconnection rate because erosion is likely ongoing during the spacecraft sampling of the MC. This simple calculation yields average reconnection rates of 0.12-0.14 mV/m at ACE and 0.19-0.22 mV/m at ST-A. Using the results of Dasso et al. [2006,2007], the average reconnection rates for the 18-20 October 1995 and 9-11 November 2004 MC events are estimated to be 0.51 and 0.45 mV/m; these are of the same order of magnitude, though somewhat higher. On average, these estimations are larger than those given in case studies of reconnection exhausts at L1 by *Davis et al.* [2006], *Phan et al.* [2006], and *Wang et al.* [2010] (0.02, 0.03 and 0.05-0.08 mV/m respectively), but as explained above this may be expected since reconnection rates ought to be larger closer to the Sun.

6. Conclusion

The present work provided a significant advancement in confirming the occurrence of MC erosion during their propagation from the Sun to the Earth, thanks to a detailed analysis of several key signatures expected to result from this process. The opportunity to observe this phenomenon from several distant vantage points with STEREO and L1 data constituted a significant asset to infer the global geometry of the MC, which was shown to be compatible with a unique large-scale flux-rope at three distant spacecraft in the heliosphere. The inferred erosion mechanism has significant potential implications for space weather since it may lead to the removal of part of the southward oriented magnetic field that impinges on Earth for some MCs. Future works also ought to quantify this possibility for all MCs of solar cycle 23.

Acknowledgements. The authors are grateful to J. Gosling, T. Phan, C. Möstl, N. Lugaz, and K. Marubashi for useful discussions. We acknowledge the use of the CDPP AMDA web-based tool, which was used for selection of the event and visualization. We are also grateful to V. Angelopoulos for the use of data from the THEMIS mission and DLR support at TU-BS for use of FGM data.

References

Acuña, M. H., D. Curtis, J. L. Scheifele, C. T. Russell, P. Schroeder, A. Szabo, J. G. Luhmann (2008), The STEREO/IMPACT Magnetic Field Experiment, *Space Science Reviews*, *136*, 203-226, doi:10.1007/s11214-007-9259-2.

Akasofu, S.-I. (1981), Energy coupling between the solar wind and the magnetosphere, *Space Science Reviews*, 28, 121-190., doi: 10.1007/BF00218810.

Al-Haddad, N., I. Roussev, et al. (2011), On the Internal Structure of the Magnetic Field in Magnetic Clouds and Interplanetary Coronal Mass Ejections: Writhe versus Twist, *The Astrophysical Journal,* 18, 2-7, doi:10.1088/2041-8205/738/2/L18.

Auster, H. U., K. H. Glassmeier, W. Magnes, O. Aydogar, W. Baumjohann, D.

627 Constantinescu, D. Fischer, et al. (2008), The THEMIS Fluxgate Magnetometer,
628 *Space Science Reviews*, *141*, 235-264, doi:10.1007/s11214-008-9365-9.

629 Borovsky, J. E., and M. H. Denton (2006), Differences between CME-driven storms and
630 CIR-driven storms, *J. Geophys. Res*., 111, A07S08, doi:10.1029/2005JA011447.

631 Bothmer, V., and R. Schwenn (1998), The structure and origin of magnetic clouds in the
632 solar wind, *Annales Geophysicae*, 16(1), 1-24, doi:10.1007/s00585-997-0001-x.

633 Burlaga, L.F., E. Sittler, F. Mariani, and R. Schwenn (1981), Magnetic loop behind an
634 interplanetary shock: Voyager, Helios, and IMP 8 observations, *J. Geophys. Res*.,
635 86(A8), 6673–6684, doi:10.1029/JA086iA08p06673.

636 Burlaga, L. F., K. W. Behannon, and L. Klein (1987), Compound Streams, Magnetic
637 Clouds and Major Geomagnetic Storms, *J. Geophys. Res*., 92(A6), 5725–5734,
638 doi:10.1029/JA092iA06p05725.

639 Burlaga, L. F. (1988), Magnetic Clouds and Force-Free Fields with Constant Alpha, *J.*
640 *Geophys. Res., 93(A7*), 7217–7224, doi:10.1029/JA093iA07p07217.

641 Crooker, N. U. (2004), Heliospheric plasma sheets, *J. Geophys. Res., 109*(A3), 1-9,
642 doi:10.1029/2003JA010170.

643 Davis, M. S., T. D. Phan, J. T. Gosling, and R. M. Skoug (2006), Detection of oppositely
644 directed reconnection jets in a solar wind current sheet, *Geophys. Res. Lett*., 33,
645 L19102, doi:10.1029/2006GL026735.

646 Dasso, S., C. H. Mandrini, P. Démoulin, M. L. Luoni (2006), A new model-independent
647 method to compute magnetic helicity in magnetic clouds, *Astronomy and*
648 *Astrophysics*, 455, 349-359, doi:10.1051/0004-6361:20064806.

649 Dasso S., Nakwacki M.S., Demoulin P., Mandrini C.H. (2007), Progressive transformation
650 of a flux rope to an ICME, *Solar Physics*, 244, 1-2, 115-137, doi: 10.1007/s11207-
651 007-9034-2, 2007.

652 Démoulin, P., and S. Dasso (2009), Magnetic cloud models with bent and oblate cross-
653 section boundaries, *Astronomy and Astrophysics,* 507(2), 969-980, doi:10.1051/0004-
654 6361/200912645.

655 Dungey, J. W. (1961), Interplanetary magnetic field and the auroral zones, *Phys. Rev. Lett.*,
656 *6*, 47-48, doi:10.1103/PhysRevLett.6.47.

657 Eriksson, S., et al. (2009), Asymmetric shear flow effects on magnetic field configuration
658 within oppositely directed solar wind reconnection exhausts, *J. Geophys. Res*., 114,
659 A07103, doi:10.1029/2008JA013990.

660 Farrugia, C., I. Richardson, L. Burlaga, R. Lepping, and V. Osherovich (1993),
661 Simultaneous observations of solar MeV particles in a magnetic cloud and in the
662 Earth's northern tail lobe: implications for the global field line topology of magnetic

clouds and for the entry of solar particles into the magnetosphere during cloud passage, *J. Geophys. Res., 98*(A9), 15497–15.

Farrugia, C. J., L. F. Burlaga, and R. P. Lepping, (1997), Magnetic Clouds and the Quiet-storm Effect at Earth, in: Magnetic Storms, Geo- R. P. Lepping et al.: A summary of WIND magnetic clouds for years 1995–2003 *phys. Monogr. Ser., 98*, edited by: B. T. Tsurutani, W. D. Gonzales, and Y. Kamide, AGU,Washington, D.C.

Farrugia, C., B. Vasquez, I. Richardson, et al. (2001), A reconnection layer associated with a magnetic cloud, *Adv. Space Res.*, 28(5), 759-764.

Farrugia, C. J., D. B. Berdichevsky, C. Möstl, A. B. Galvin, M. Leitner, M. A. Popecki, K. D. C. Simunac, et al. (2011), Multiple, distant (40°) in situ observations of a magnetic cloud and a corotating interaction region complex, *Journal of Atmospheric and Solar-Terrestrial Physics*, 73, 1254-1269, doi:10.1016/j.jastp.2010.09.011.

Foullon, C., C. J. Owen, S. Dasso, L. M. Green, I. Dandouras, H. a. Elliott, a. N. Fazakerley, Y. V. Bogdanova, and N. U. Crooker (2007), Multi-Spacecraft Study of the 21 January 2005 ICME, *Solar Physics*, *244*(1-2), 139-165, doi:10.1007/s11207-007-0355-y.

Foullon, C. et al. (2009), The Apparent Layered Structure of the Heliospheric Current Sheet: Multi-Spacecraft Observations, *Solar Physics*, *259*(1-2), 389-416, doi:10.1007/s11207-009-9452-4.

Fujimoto, M., W. Baumjohann, K. Kabin, R. Nakamura, J. A. Slavin, N. Terada and L. Zelenyi (2007), Hermean magnetosphere-solar wind interaction, *Space Sci. Rev*., 132, 2-4, 529-550, doi: 10.1007/s11214-007-9245-8.

Galvin, A. B. et al. (2008), The Plasma and Suprathermal Ion Composition (PLASTIC) Investigation on the STEREO Observatories, *Space Science Reviews*, *136*(1-4), 437-486, doi:10.1007/s11214-007-9296-x.

Goldstein, H. (1983), On the field configuration in magnetic clouds, in Solar Wind Five, edited by Neugebauer, M., *NASA Conf. Publ.*, CP-2280, 731–733.

Gopalswamy, N., S. Yashiro, and S. Akiyama (2007), Geoeffectiveness of halo coronal mass ejections, *J. Geophys. Res.,* 112, A06112, doi:10.1029/2006JA012149.

Gosling, J. T., D. Baker, S. Bame, W. Feldman, R. Zwickl, E. Smith (1987), Bidirectional Solar Wind Electron Heat Flux Events, *J. Geophys. Res*., 92(A8), 8519–8535, doi:10.1029/JA092iA08p08519.

Gosling, J. T. (1990), Coronal mass ejections and magnetic flux ropes in interplanetary space, in Physics of Magnetic Flux Ropes, *Geophys. Monogr. Ser.*, vol. 58, edited by C. T. Russell, E. R. Priest, and L. C. Lee, pp. 343–364, AGU, Washington, D. C.

Gosling, J. T. (1993), The Solar Flare Myth, *J. Geophys. Res*., 98(A11), 18,937–18,949, doi:10.1029/93JA01896.

700 Gosling, J. T., R. Skoug, W. Feldman, D. McComas (2002), Symmetric suprathermal
701 electron depletions on closed field lines in the solar wind, *Geophys. Res. Lett.*, 29(12),
702 1573, doi:10.1029/2001GL013949.

703 Gosling, J. T., R. M. Skoug, D. J. McComas, and C. W. Smith (2005a), Direct evidence for
704 magnetic reconnection in the solar wind near 1 AU, *J. Geophys. Res.*, 110, A01107,
705 doi:10.1029/2004JA010809.

706 Gosling, J. T., R. M. Skoug, D. J. McComas, and C. W. Smith (2005b), Magnetic
707 disconnection from the Sun: Observations of a reconnection exhaust in the solar wind
708 at the heliospheric current sheet, *Geophys. Res. Lett.*, 32, L05105,
709 doi:10.1029/2005GL022406.

710 Gosling, J. T., S. Eriksson, R. Schwenn (2006a), Petschek-type magnetic reconnection
711 exhausts in the solar wind well inside 1 AU: Helios, *J. Geophys. Res.*, 111, A10102,
712 doi:10.1029/2006JA011863.

713 Gosling, J. T., D. J. McComas, R. M. Skoug, and C. W. Smith (2006b), Magnetic
714 reconnection at the heliospheric current sheet and the formation of closed magnetic
715 field lines in the solar wind, Geophys. Res. Lett., 33, L17102,
716 doi:10.1029/2006GL027188.

717 Gosling, J. T., S. Eriksson, L. M. Blush, T. D. Phan, J. G. Luhmann, D. J. McComas, R. M.
718 Skoug, M. H. Acuna, C. T. Russell, and K. D. Simunac (2007), Five spacecraft
719 observations of oppositely directed exhaust jets from a magnetic reconnection X-line
720 extending $> 4.26 \times 10^6$ km in the solar wind at 1 AU, *Geophys. Res. Lett.*, 34, L20108,
721 doi:10.1029/2007GL031492.

722 Gosling, J. T., A. Szabo, (2008), Bifurcated current sheets produced by magnetic
723 reconnection in the solar wind, *J. Geophys. Res.*, 113, A10103,
724 doi:10.1029/2008JA013473.

725 Gulisano, A., S. Dasso, C. Mandrini, P. Démoulin (2007), Estimation of the bias of the
726 Minimum Variance technique in the determination of magnetic clouds global
727 quantities and orientation, *Advances in Space Research*, *40*, 1881-1890,
728 doi:10.1016/j.asr.2007.09.001.

729 Howard, T. A., and S. J. Tappin (2009), Interplanetary Coronal Mass Ejections Observed
730 in the Heliosphere: 3. Physical Implications, *Space Science Reviews*, *147*(1-2), 89-110,
731 doi:10.1007/s11214-009-9577-7.

732 Hudson, P. D. (1970), Discontinuities in an anisotropic plasma and their identification in
733 the solar wind, *Planet. Space Sci.*, 19, 1161.

734 Huttunen, K. E. J., S. D. Bale, and C. Salem (2008), Wind observations of low energy
735 particles within a solar wind reconnection region, *Ann. Geophys*, 26, 2701-2710.

736 Kaiser, M. L., T. A. Kucera, J. M. Davila, O. C. St. Cyr, M. Guhathakurta, E. Christian
737 (2008), The STEREO Mission: An Introduction, *Space Science Reviews*, *136*(1-4), 5-
738 16, doi:10.1007/s11214-007-9277-0.

739 Kawano, H., T. Higuchi (1995), The bootstrap method in space physics: Error estimation
740 for the minimun variance analysis, *Geophys*. *Res*. *Lett*., 22(3), 307–310,
741 doi:10.1029/94GL02969.

742 Klein, L. W., and L. F. Burlaga (1982), Interplanetary magnetic clouds at 1 AU, *J*.
743 *Geophys*. *Res*., 87(A2), 613–624, doi:10.1029/JA087iA02p00613.

744 Kilpua, E. K. J., L. K. Jian, Y. Li, J. G. Luhmann, and C. T. Russell (2011), Multipoint
745 ICME encounters: Pre-STEREO and STEREO observations, *Journal of Atmospheric*
746 *and Solar-Terrestrial Physics*, 73, 1228-1241, doi:10.1016/j.jastp.2010.10.012.

747 Lavraud, B., and J. E. Borovsky (2008), Altered solar wind-magnetosphere interaction at
748 low Mach numbers: Coronal mass ejections, *J. Geophys. Res.*, 113, A00B08,
749 doi:10.1029/2008JA013192.

750 Lavraud, B., J. T. Gosling, A. P. Rouillard, A. Fedorov, A. Opitz, J.-A. Sauvaud, C.
751 Foulllon, I. Dandouras, V. Génot, C. Jacquey, P. Louarn, C. Mazelle, E. Penou, T. D.
752 Phan, D. Larson, J. G. Luhmann, P. Schroeder, R. M. Skoug, J. T. Steinberg and C. T.
753 Russell (2009), Observation of a complex solar wind reconnection exhaust from
754 spacecraft separated by over 1800 RE, *Solar Phys*., 256, No. 1-2, p. 379-392,
755 doi:10.1007/s11207-009-9341-x.

756 Lavraud, B., A. Opitz, J. T. Gosling, A. P. Rouillard, K. Meziane, J.-A. Sauvaud, A.
757 Fedorov, I. Dandouras, V. Génot, C. Jacquey, P. Louarn, C. Mazelle, E. Penou, D. E.
758 Larson, J. G. Luhmann, P. Schroeder, L. Jian, C. T. Russell, C. Foullon, R. M. Skoug,
759 J. T. Steinberg, K. D. Simunac, and A. B. Galvin (2010), Statistics of counter-
760 streaming solar wind suprathermal electrons at solar minimum: STEREO
761 observations, *Ann. Geophys*., 28, 233-246.

762 Lavraud, B., M. J. Owens, and A. P. Rouillard (2011), In situ signatures of interchange
763 reconnection between magnetic clouds and open magnetic fields: A mechanism for the
764 erosion of polar coronal holes?, *Solar Phys*., 270(1), 285-296, doi:10.1007/s11207-
765 011-9717-6.

766 Lepping, R. P., J. A. Jones, L. F. Burlaga (1990), Magnetic Field Structure of Interplanetary
767 Magnetic Clouds at 1 AU, *J*. *Geophys*. *Res*., 95(A8), 11,957–11,965,
768 doi:10.1029/JA095iA08p11957.

769 Luhmann, J. G. et al. (2008), STEREO IMPACT Investigation Goals, Measurements, and
770 Data Products Overview, *Space Science Reviews*, *136*(1-4), 117-184,
771 doi:10.1007/s11214-007-9170-x.

772 Lundquist, S. (1950), Magneto-hydrostatic fields. *Arkiv Fysik*, Bd 2, nr 35.

773 Marubashi, K. (1986), Structure of the interplanetary magnetic clouds and their solar
774 origins, *Adv. Space Res.*, 6, 335–338.

775 Mandrini C.H., Pohjolainen S., Dasso, S., Green, L.M, Démoulin P., van Driel-Gesztelyi
776 L., Copperwheat, C., Foley, C. (2005), Interplanetary flux rope ejected from an X-ray
777 bright point. The smallest magnetic cloud source-region ever observed, A&A, 434,

725, doi: *10.1051/0004-6361:20041079.*

McComas, D., S. Bame, P. Barker, W. Feldman, J. Phillips, P. Riley, and J. Griffee (1998), Solar Wind Electron Proton Alpha Monitor (SWEPAM) for the Advanced Composition Explorer, *Space Science Reviews*, *86*(1), 563–612.

McFadden, J. P., Carlson, C. W., Larson, D., Ludlam, M., Abiad, R., Elliott, B., Turin, P., et al. (2008), The THEMIS ESA Plasma Instrument and In-flight Calibration, *Space Science Reviews*, *141*, 277-302, doi:10.1007/s11214-008-9440-2.

Möstl, C., C. Miklenic, C. J. Farrugia, M. Temmer, A. Veronig, A. B. Galvin, H. K. Biernat, and H. Observatory (2008), Two-spacecraft reconstruction of a magnetic cloud and comparison to its solar source, *Ann. Geophys.*, 26, 3139-3152.

Möstl, C., M. Temmer, T. Rollett, C. J. Farrugia, Y. Liu, A. M. Veronig, M. Leitner, A. B. Galvin, and H. K. Biernat (2010), STEREO and Wind observations of a fast ICME flank triggering a prolonged geomagnetic storm on 5–7 April 2010, Geophys. Res. Lett., 37, L24103, doi:10.1029/2010GL045175.

Nakwacki, M., S. Dasso, C. Mandrini, and P. Démoulin (2008); Analysis of large scale MHD quantities in expanding magnetic clouds, *Journal of Atmospheric and Solar-Terrestrial Physics*, *70*(10), 1318-1326, doi:10.1016/j.jastp.2008.03.006.

Owens, M. J., and N. U. Crooker (2006), Coronal mass ejections and magnetic flux buildup in the heliosphere, *J. Geophys. Res.*, 111, A10104, doi:10.1029/2006JA011641.

Owens, M. J., P. Démoulin, N. P. Savani, B. Lavraud, and A. Ruffenach (2012), Implications of non-cylindrical flux ropes for magnetic cloud reconstruction techniques and the interpretation of double flux-rope events, *Solar Physics*, doi: 10.1007/s11207-012-9939-2, (In Press).

Paschmann, G., I. Papamastorakis, W. Baumjohann, N. Sckopke, C. W. Carlson, B. U. Ö. Sonnerup, and H. Lühr (1986), The Magnetopause for Large Magnetic Shear: AMPTE/IRM Observations, *J. Geophys. Res.*, 91(A10), 11,099–11,115, doi:10.1029/JA091iA10p11099.

Phan, T. D., J. T. Gosling, M. S. Davis, R. M. Skoug, M. Øieroset, R. P. Lin, R. P. Lepping, et al. (2006), A magnetic reconnection X-line extending more than 390 Earth radii in the solar wind, *Nature*, *439*(7073), 175-8, doi:10.1038/nature04393.

Qiu, J., Q. Hu, T. A. Howard, and V. B. Yurchyshyn (2007), On the magnetic flux budget in low-corona magnetic reconnection and interplanetary coronal mass ejections*, The Astrophysical Journal,* 659*,* 758-772.

Richardson, I. G., and H. V. Cane (2010), Near-Earth Interplanetary Coronal Mass Ejections During Solar Cycle 23 (1996 – 2009): Catalog and Summary of Properties, *Solar Physics*, *264*(1), 189-237, doi:10.1007/s11207-010-9568-6.

Rouillard, a. P., B. Lavraud, N. R. Sheeley, J. a. Davies, L. F. Burlaga, N. P. Savani, C. Jacquey, and R. J. Forsyth (2010), White Light and in Situ Comparison of a Forming

816 Merged Interaction Region, *The Astrophysical Journal*, *719*(2), 1385-1392,
817 doi:10.1088/0004-637X/719/2/1385.

818 Sauvaud, J.-A, D. Larson, C. Aoustin, D. Curtis, J.-L. Médale, A. Fedorov, J. Rouzaud, et
819 al. (2008), The IMPACT Solar Wind Electron Analyzer (SWEA), *Space Science*
820 *Reviews*, *136*, 227-239, doi:10.1007/s11214-007-9174-6.

821 Schmidt, J. M., and P. J. Cargill (2003), Magnetic reconnection between a magnetic cloud
822 and the solar wind magnetic field, *J. Geophys. Res*, 108(A1), 1-10,
823 doi:10.1029/2002JA009325.

824 Shodhan, S., N. U. Crooker, S. W. Kahler, R. J. Fitzenreiter, D. E. Larson, R. P. Lepping,
825 G. L. Siscoe, and J. T. Gosling (2000), Counterstreaming electrons in magnetic clouds,
826 *J. Geophys. Res.*, 105(A12), 27261, doi:10.1029/2000JA000060.

827 Skoug, R. M., J. T. Gosling, D. J. McComas, C. W. Smith, and Q. Hu (2006), Suprathermal
828 electron 90° pitch angle depletions at reverse shocks in the solar wind, J. Geophys.
829 Res., 111, A01101, doi:10.1029/2005JA011316.

830 Smith, C. W., J. L'Heureux, N. F. Ness, M. H. Acuña, L. F. Burlaga, and J. Scheifele
831 (1998), The ACE magnetic fields experiment, *Space Science Reviews*, *86*, 613–632.

832 Sonnerup, B. U. Ö., L. J. Cahill (1967), Magnetopause Structure and Attitude from
833 Explorer 12 Observations, *J. Geophys. Res.*, 72(1), 171–183,
834 doi:10.1029/JZ072i001p00171.

835 Steinberg, J. T., J. T. Gosling, R. M. Skoug, and R. C. Wiens (2005), Suprathermal
836 electrons in high-speed streams from coronal holes: Counterstreaming on open field
837 lines at 1 AU, J. Geophys. Res., 110, A06103, doi:10.1029/2005JA011027.

838 Stone, E., A. Frandsen, R. Mewaldt, E. Christian, D. Margolies, J. Ormes, and F. Snow
839 (1998), The Advanced Composition Explorer, *Space Science Reviews*, *86*, 1–22.

840 Taubenschuss, U., N. V. Erkaev, H. K. Biernat, C. J. Farrugia, C. Möstl, and U. V.
841 Amerstorfer (2010), The role of magnetic handedness in magnetic cloud propagation,
842 *Annales Geophysicae*, 28(5), 1075-1100, doi:10.5194/angeo-28-1075-2010.

843 Vandas, M.; Fischer, S.; Pelant, P.; Geranios, A. (1993), Evidence for a spheroidal structure
844 of magnetic clouds, *Journal of Geophysical Research,* 98, 21,061-21,069, doi :
845 10.1029/93JA01749.

846 Wimmer-Schweingruber, R. F., N. U. Crooker, A. Balogh, V. Bothmer, R. J. Forsyth, P.
847 Gazis, J. T. Gosling, et al. (2006), Understanding Interplanetary Coronal Mass Ejection
848 Signatures, *Space Science Reviews*, *123*, 177-216, doi:10.1007/s11214-006-9017-x.

849 Wang, Y., F. Wei, X. Feng, S. Zhang, P. Zuo, and T. Sun (2010), Energetic Electrons
850 Associated with Magnetic Reconnection in the Magnetic Cloud Boundary Layer,
851 *Physical Review Letters*, 105(19), doi:10.1103/PhysRevLett.105.195

852

A. Ruffenach, Institut de Recherche en Astrophysique et Planétologie, 9 Avenue du Colonel Roche, BP 44346, 31028 Toulouse Cedex 4, France. (Alexis.ruffenach@irap.omp.eu)

FIGURE CAPTIONS:

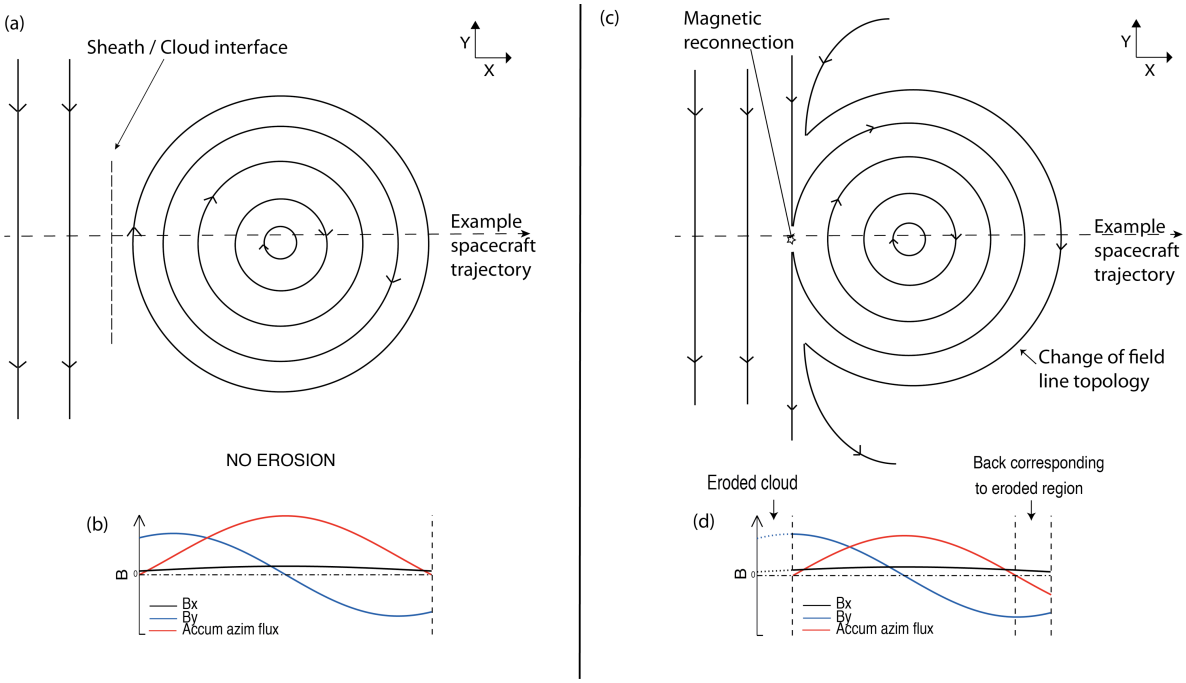

Figure 1. Schematic representing the magnetic structure of non-eroded (a) and eroded (c) MCs together with the expected variations in the magnetic field components and accumulated azimuthal flux (b and d). The analysis needs to be made in the proper MC coordinate system as is implicit here.

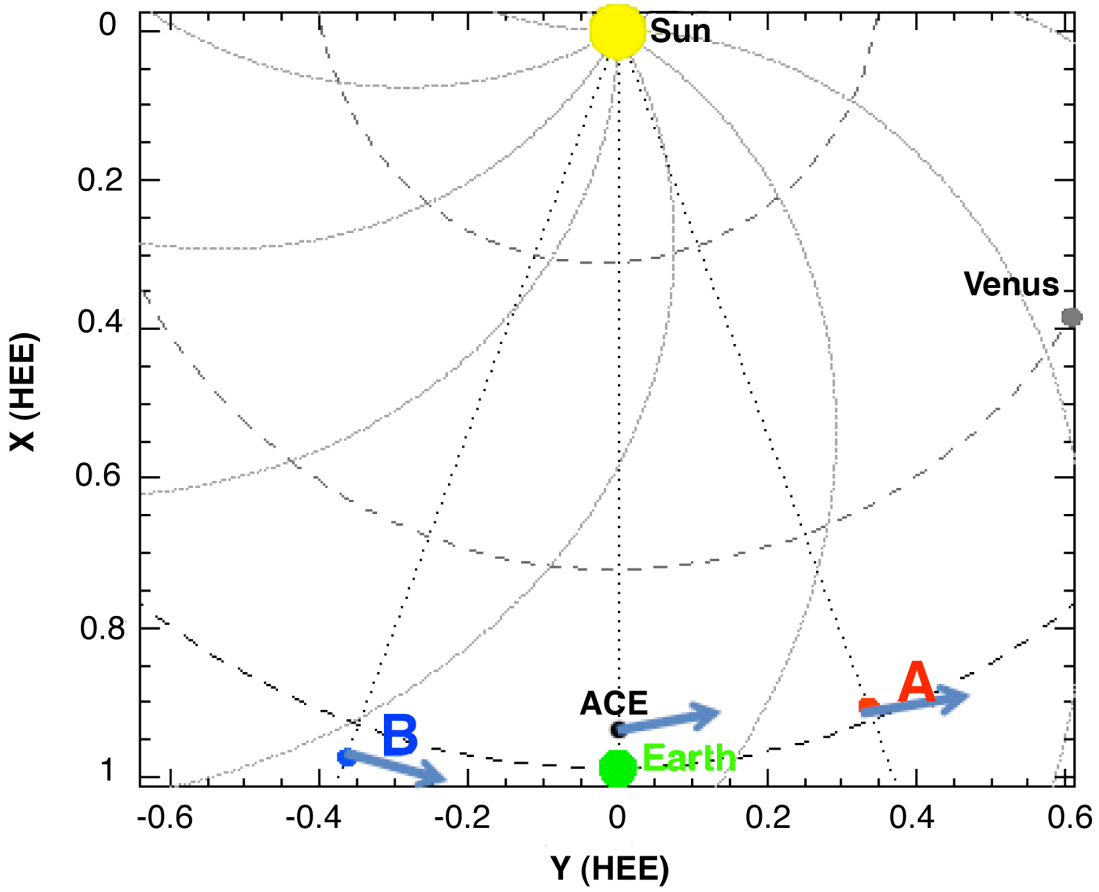

Figure 2. ACE, ST-A, ST-B, and Earth locations on November 19-20, 2007 in the ecliptic plane with the respective projection of MC axis orientations inferred from MVA analysis.

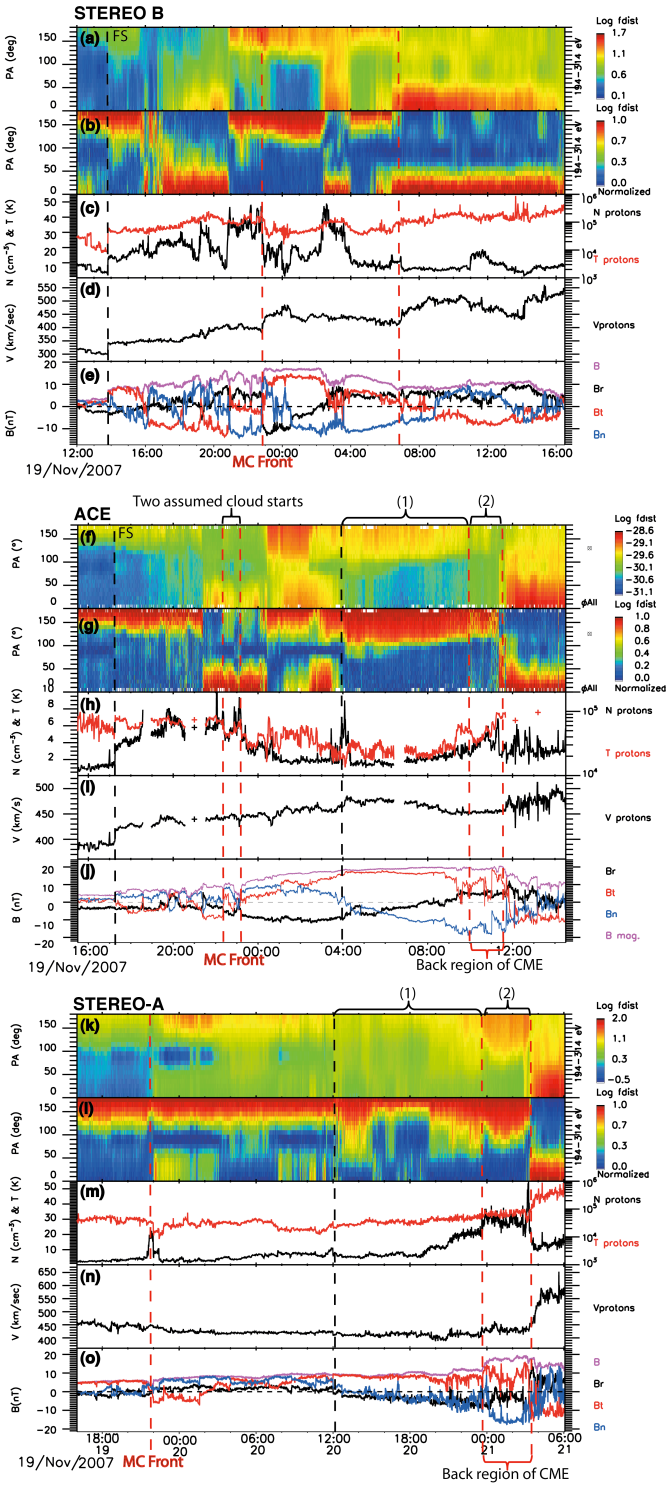

Figure 3. Plasma and magnetic field data from ST-B, ACE, and ST-A during the period 19-21 November 2007. The various MC boundaries used are marked with red dashed lines (see text for details). The panels (a/f/k) show the suprathermal electron pitch angle distributions, (b/g/l) the normalized (between 0 and 1 for each time sample) pitch angle distributions, (c/h/m) the proton temperature (red line) and proton density (black line), (d/i/n) the proton speed, and (e/j/o) the magnetic field components in RTN coordinates. Region (1) corresponds to the open MC region interpreted as resulting from interchange reconnection at the Sun. Region (2) is deemed to be the back region resulting from erosion. It also shows unidirectional electrons but with markedly different strahl properties (cf. Figure 9). Forward shocks (FS) are shown with a dashed line at ACE and ST-B.

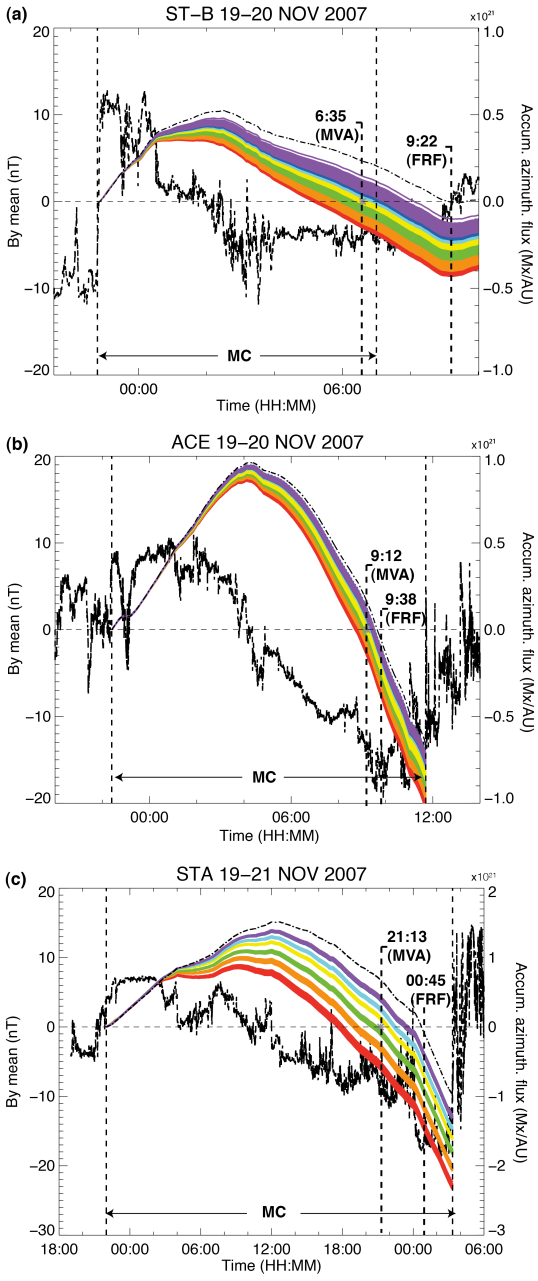

Figure 4. B_{ycloud} component and accumulated azimuthal magnetic flux per unit length for ST-B (a), ACE (b), and ST-A (c). The colored curves show the results using orientations deduced from MVA with bootstrap method applied to different intervals (cf. Section 4.1.2). The dash-dotted curves show the results using the orientation deduced from force-free MC fitting. Vertical lines indicate the boundaries of the MC and the time at which the azimuthal flux is balanced (cuts zero) for both the (mean of) MVA and FRF methods. Cf. also Table 1 for details.

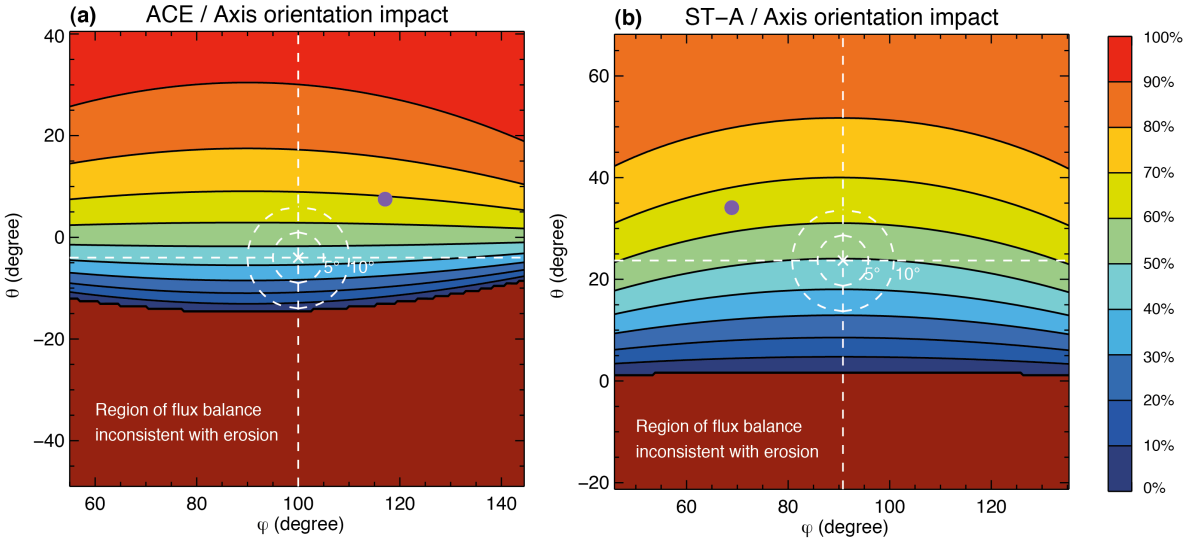

Figure 5. Parametric study of the impact of an arbitrary MC axis orientation on the amount of azimuthal magnetic flux eroded from the front of the MC at ACE (a) and ST-A (b), as defined in Section 4.1.4. The display is centered on the orientation given by the mean MC axis orientation from our analyses (Cf. Table 1). The line separating the dark blue and the brown regions in the plots corresponds to axes orientations for which the azimuthal flux is exactly balanced (in the front and back parts of the MC). Regions with other colors (blue to red) are consistent with erosion of various degrees (cf. color scale for MC flux erosion percentage), while the entire brown part of the plot is inconsistent with erosion and the presence of a back region. The axis orientation obtained by *Farrugia et al*. [2011] using MVA (from WIND and ST-A) is given as a solid purple circle for context.

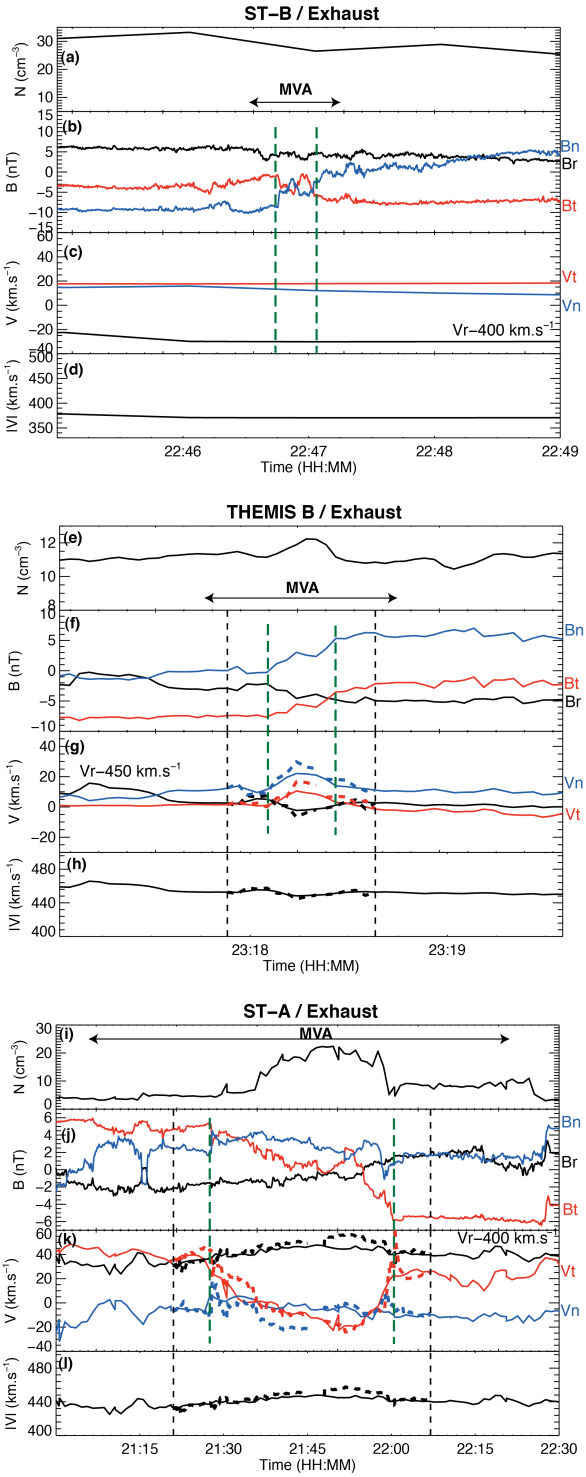

Figure 6. Data for the exhausts seen at ST-B, THEMIS-B and ST-A at the front of the MC together with Walén test results when the time resolution is sufficient (THEMIS-B and ST-A). For each spacecraft the panels show: (a/e/i) Proton density, (b/f/j) magnetic field components, (c/g/k) proton velocity components observed and predicted (dashed lines), and (d/h/j) proton velocity magnitude observed and predicted (dashed lines). The two black vertical lines denote the reference times for the Walén test (which is performed "inward"). The green vertical lines denote the edges of the exhaust, i.e., the bifurcated current sheets. The time interval used to determine the orientation of the reconnection line through MVA is also indicated with an arrow (Cf. Table 2).

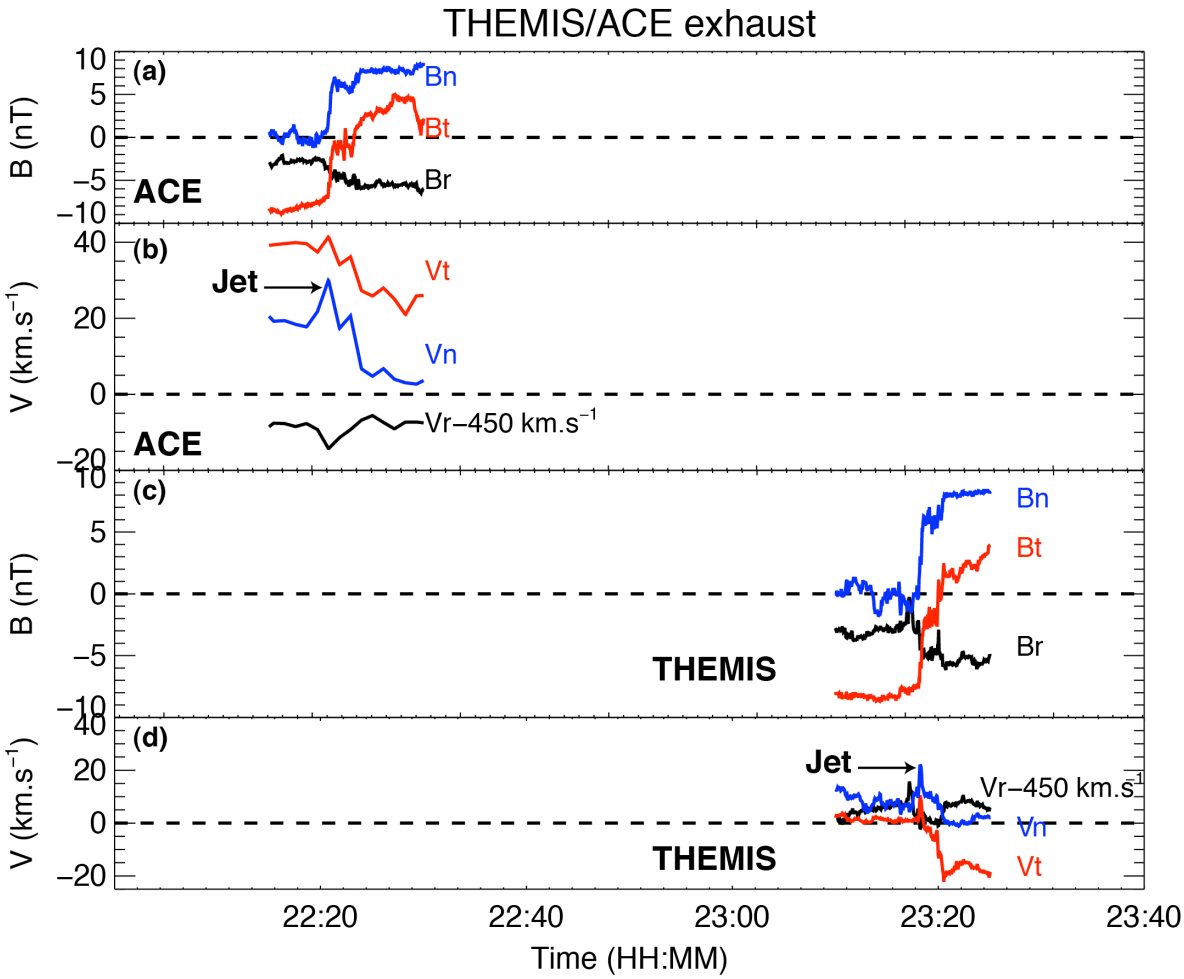

Figure 7. Data for the exhaust seen at ACE and THEMIS-B at the MC front boundary on 19 November. Panels (a) and (c) show the magnetic field components for ACE and THEMIS, respectively. Panels (b) and (d) show the associated velocity components. Despite a resolution too low to allow a proper Walén test, a proton jet is clearly also observed at ACE at the front boundary of the MC.

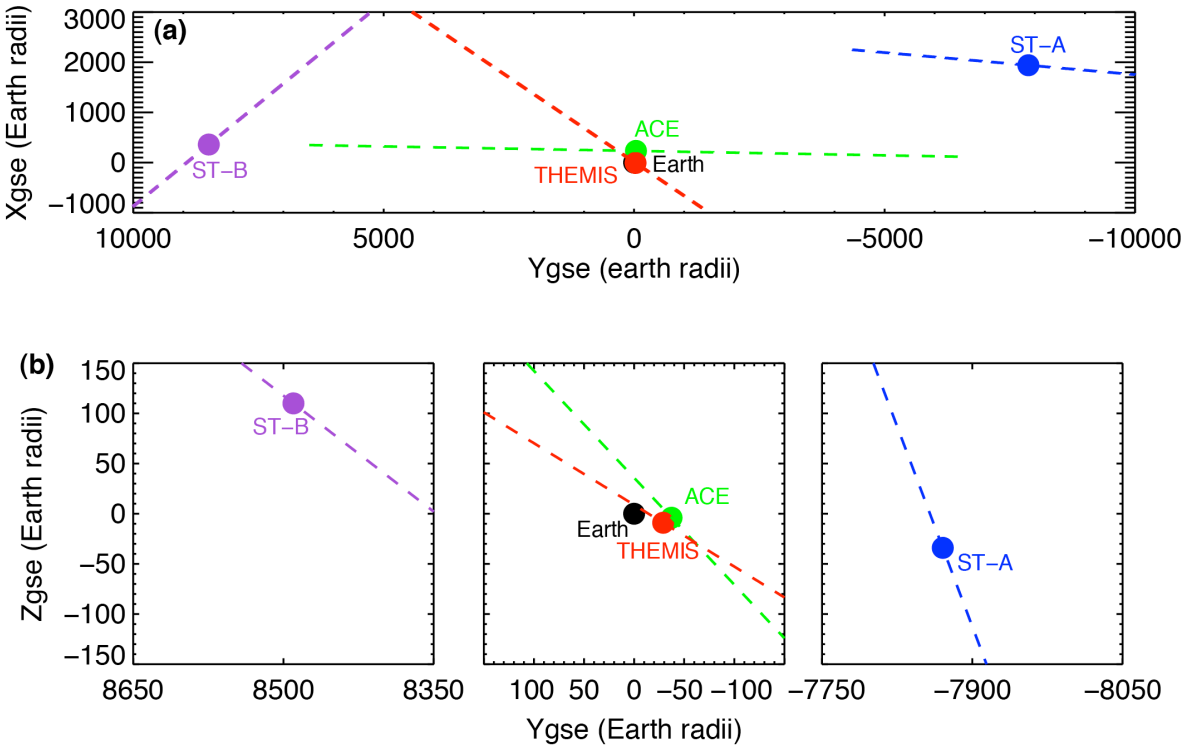

Figure 8. Projections of the reconnection line orientations at each spacecraft in GSE coordinates at 22:00 UT on 19 November 2007 in the X-Y_{GSE} (a) and Z-Y_{GSE} (b) planes.

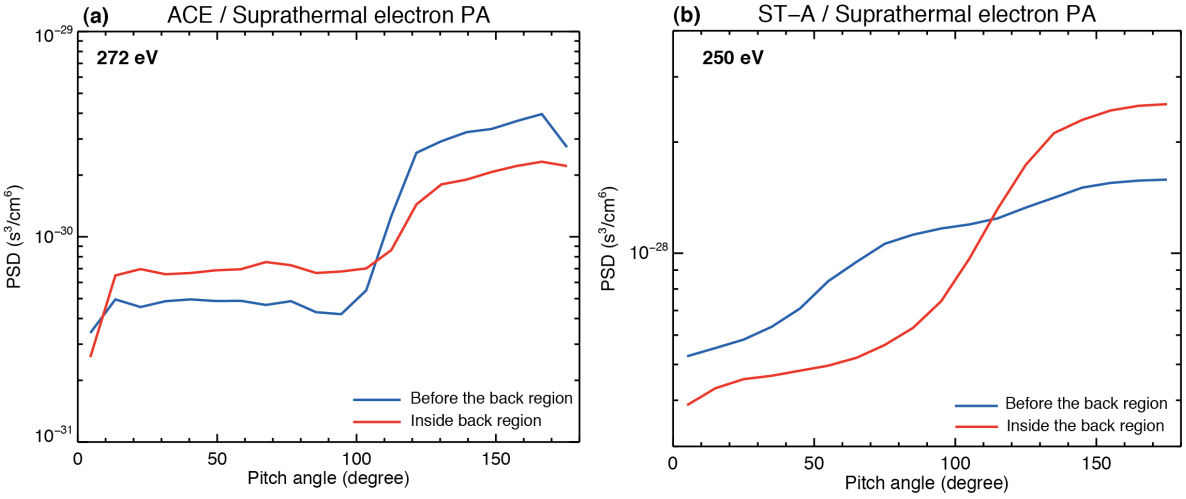

Figure 9. ACE (a) and ST-A (b) suprathermal electron pitch angle distributions obtained in the MC back region (red curve) and the MC core (blue curve), at times close to the boundary separating those two regions (see section 4.4 for details). Each is an average of consecutive PAD samples over 5 minutes.

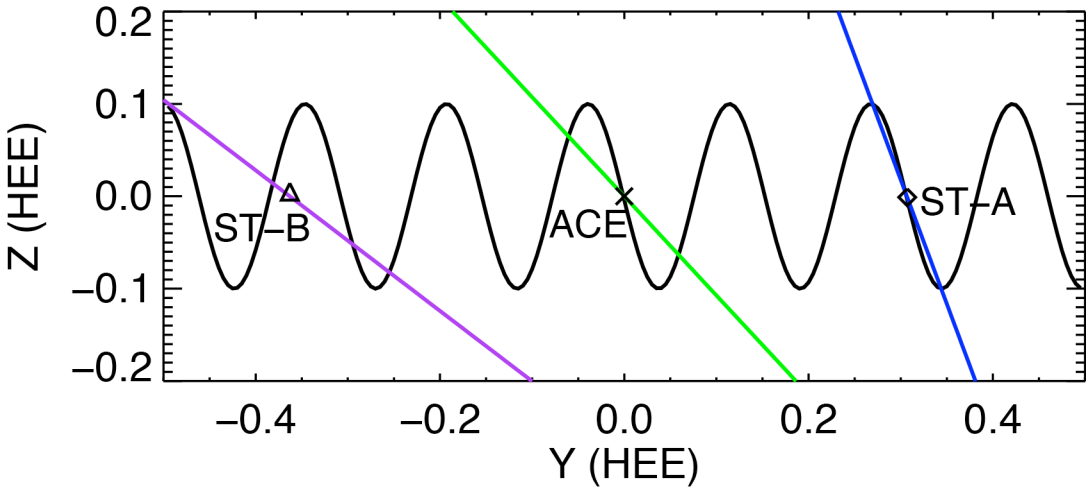

Figure 10. Illustration of the projected helical MC field (black curve), with estimated reconnection line orientations (color curves), for the exhausts observed at the MC front boundaries at the three spacecraft in the ZY planes (HEE coordinates). This suggests that it may not be the same reconnection line observed at all spacecraft.

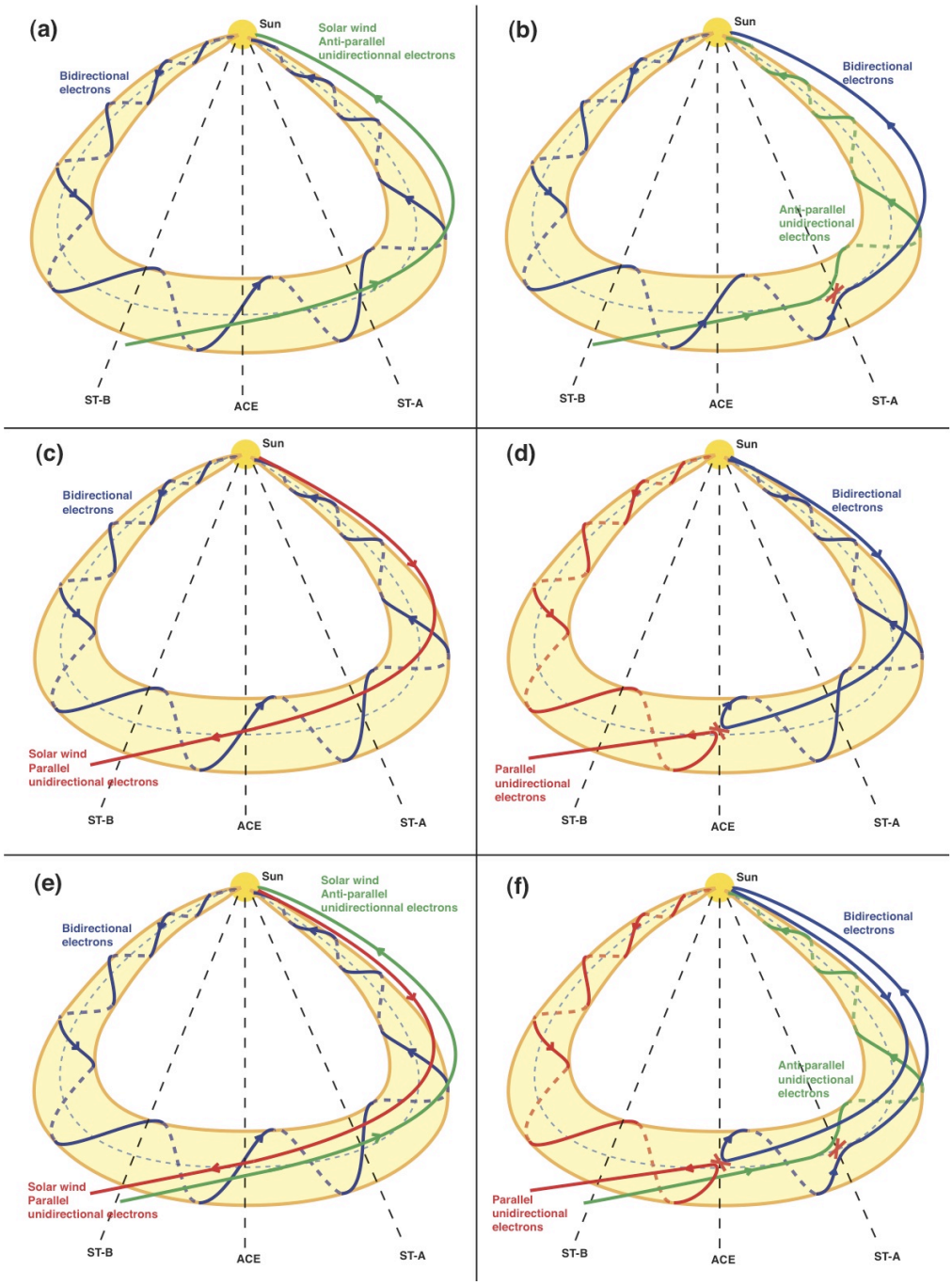

Figure 11. Illustration of different reconnection scenarios at the front of the MC and resulting global three-dimensional topologies. Panels a, c and e depict the topology of the MC and solar wind magnetic field lines before magnetic reconnection occurs. Panels b, d and f represent the global magnetic field topology that may be inferred in the case when magnetic reconnection occurs at ST-A (b), ACE (d) and at both spacecraft (f). Reconnection is assumed with solar wind from a toward sector at ST-A and an away sector at ACE, as observed. Blue lines correspond to closed magnetic field lines where counter-streaming suprathermal electron beams may be expected. Green and red lines respectively correspond to open field lines with anti-parallel and parallel unidirectional suprathermal electrons. Arrows show the orientation of the magnetic field. These topologies, and inferred electron properties, must be viewed as highly idealized and thus not realistic. Much more complex, and thus unpredictable, configurations may be expected as a function of the type and spatio-temporal variability of reconnection lines at the MC front boundary.

TABLES:

	ACE	ST-A	ST-B
MVA and cloud-fitting time interval	23:13 (19 Nov.)-11:42 (20 Nov.)	22:00 (19 Nov.)-3:20 (21 Nov.)	22:52 (19 Nov.)-7:00 (20 Nov.)
Azimuthal flux integration start time	22:22 (19 Nov.)	22:00 (19 Nov.)	22:47 (19 Nov.)
MC axis orientation from the mean of all MVA results (with standard deviations)	θ=-3°±1° φ=101.5°±0.4°	θ=31°±7° φ=84°±6°	θ=-39°±4° φ=96°±8°
MC axis orientation from FRF	θ=-5° φ=99°	θ=17° φ=97°	θ=-50° φ=92°
MC axis orientation: mean of results from MVA and FRF methods	θ=-4° φ=100°	θ=24° φ=91°	θ=-45° φ=94°
Start of back region inferred from electron PAD	9:53 (20 Nov.)	23:40 (20 Nov.)	/
Time of flux balance (mean of results from MVA and FRF methods)	9:26±13min (20 Nov.)	22:59± 1:48 (20 Nov.)	7:58±1:23 (20 Nov.)
Intermediate/minimum eigenvalue ratio (mean from all MVA analyses)	11.3	6.31	6.32
Impact parameter from FRF (positive means spacecraft crosses north of MC center axis)	0.18	0.03	-0.11
Alpha parameter from FRF	2.16	2.39	1.94

Table 1. Summary of the results obtained for the azimuthal flux balance-related analyses at each spacecraft.

	ACE	THEMIS	ST-A	ST-B
Time interval of exhaust location	22:20:30-22:21:30	23:18:05-23:18:26	21:28 – 22:01	22:46:45-22:47:03
Time interval of MVA	22:19:30-22:22:30	23:17:44-23:18:47	21:13-22:16	22:46:36-22:47:12
Reconnection line orientation (GSE)	[-0.01, -0.68, -0.73]	[-0.49, -0.74, -0.45]	[-0.03, -0.35, -0.94]	[0.54, -0.67, -0.51]
Walén Test	Insufficient resolution	ok	ok	Insufficient resolution
Magnetic shear angle	72.5°	73.0°	142.8°	62°

Table 2. Properties of the exhausts observed at the MC front boundaries at each spacecraft.